Effect of surface preparation on the corrosion of austenitic stainless steel 304L in high temperature steam and simulated PWR primary water

Sarata Cissé [a], Lydia Laffont [b,*], Benoit Tanguy [a], Marie-Christine Lafont [b], Eric Andrieu [b]

[a] Nuclear Material Department, CEA Saclay, 91191 Gif sur Yvette, France
[b] Institut CARNOT, CIRIMAT-ENSIACET, 4 allée Emile Monso, 31030 Toulouse Cedex 4, France

A B S T R A C T

The corrosion behavior of 304L grade stainless steel (SS) in high-temperature steam and in a simulated Pressurized Water Reactor (PWR) is studied. The goal was to characterize the nature of the oxide coating generated during 500 h exposure of samples in a 400 °C steam (200 bar) or a 340 °C simulated PWR. Accelerating the effect of the steam environment as well as the influence of surface preparation have been studied. Two initial sample surfaces were used: mechanical polishing and finishing grinding. Oxide coatings were investigated using TEM imaging coupled with EELS spectroscopy and R – SIMS (Secondary Ion Mass Spectroscopy).

Keywords:
A. Stainless steel
B. TEM
B. SIMS
C. Oxide coatings

1. Introduction

Austenitic stainless steels owe their high corrosion resistance in aqueous solutions to the presence of a thin oxide film at the surface referred to as the passive film. The corrosion kinetics is slowed down by the passive film which acts as a protective barrier for the alloy. It was reported by Bloom et al. [1] that in neutral and alkaline solutions in ampoules, the thin monolayer film grows following a logarithmic time law. Conversely, Potter and Mann [2] found that in similar solutions but in autoclaves, a duplex film is formed during oxidation which grows following a parabolic time law. Actually, at low temperatures, the passive film is very thin and measures only a few nanometers while oxide thickness increases as temperature increases, with the formation of a second layer made of outer crystallites rich in iron. Numerous studies [3–11] have reported the duplex oxide layer and describe these crystallites as spinels, which are of the AB_2O_4 crystallite type (with A = Fe (II) or Ni (II), B = Fe (III) or Cr (III)). The oxide layer is so constituted as follows [11]:

1. The inner layer with fine-grained oxide, compact and very adherent to base metal. This layer is generally nonporous, very protective and chromium rich.
2. The external layer is composed of non-uniform large grains, which have precipitated from the solution.

Amongst others Terachi [7] reported, for 316 stainless steel under PWR nominal solution, a duplex structure layer: a compact inner layer composed of $FeCr_2O_4$ spinels and a coarse–grained outer layer made of Fe_3O_4 spinels.

The boundary between the inner layer and the outer layer lies at the initial metal/solution interface. Thus the inner layer grows at the base metal/oxide interface and the outer layer grows at the oxide–solution interface [6]. It is reported that the inner layer retains the more protective components, such as Cr due their low diffusion kinetics. It is generally agreed that oxide films are formed by diffusion of Fe to the outer layer and diffusion of O from solution to the alloy through the inner layer. Ni enrichment has also been observed at the metal/oxide interface [7].

The oxide layer actually grows by diffusion mechanisms including ionic species present in the metal and aqueous ions from solution. Thus, to understand the growth of these oxide layers, numerous models have been proposed including models with layer growth as the rate-limiting step. Overall, three main diffusion mechanisms have been considered:

1. Solid state diffusion of species through the solid oxide [12].
2. Diffusion of species from the liquid through the pores present in the passive layer [4].
3. Diffusion of species through grain boundaries [6].

For any particular environment, it is then of interest to accurately characterize the microstructure of the oxide layer in order to assess which type of model best explains the growth of the oxide film.

* Corresponding author. Tel.: +33 534323437; fax: +33 534323498.
E-mail address: lydia.laffont@ensiacet.fr (L. Laffont).

This study is dedicated to microstructural characterization of the oxide layer resulting from exposition of 304L SS samples in high temperature steam and simulated nominal PWR water. The objectives of the work were the following:

1. To identify the nature of the components present in the oxide film formed on samples exposed to steam and simulated nominal PWR environments.
2. To study the influence of initial surface preparation by oxidizing polished samples and ground samples. Surface preparation is important because microstructural modifications at the surface may impact electrochemical mechanisms. In fact, several authors [13–17] have pointed the influence of surface roughness on corrosion resistance (electropolishing seems to be one of the best ways to remove roughness).
3. To estimate the accelerating effect of a critical environment such as steam with regard to simulated nominal PWR environment. For this purpose, the representativeness of corrosion products formed in the steam compared to a simulated nominal PWR environment will be qualified.

The results will give an insight into the surface reactivity of 304L stainless steel and should allow the prevention of the mechanisms occurring during production and degradation of protective passive film.

2. Experimental methods

The material studied is a 304L austenitic stainless steel provided as a plate which was solution-treated at 950 °C for 30 min then water-quenched. Chemical analyses were carried out by means of GDMS (Glow Discharge Mass Spectroscopy) analysis. The chemical composition of the alloy is shown in Table 1.

2.1. Surface preparation

Two sets of rectangular samples (L = 20 mm, W = 20 mm, T = 2 mm) were considered in the study: the first set of samples referred to as "H1" was machined by Electric Discharge Machining (EDM) also named spark machining, from the thickness of the plate. The samples were ground on both sides by SiC papers of grades from 250 to 4000, then polished using diamond pastes (from 3 to 1 μm) until a mirror surface and finally subjected to a mechanical/chemical polishing using a colloidal silica suspension (named OP-S for 'Oxide Polishing-Silica' by Struers). Finally the samples were carefully cleaned in ethanol.

The second set of samples referred to as "H2" was first spark machined from the thickness of the plate and then finished by precision grinding. No additional polishing was applied to set H2.

Half of the samples from sets H1 and H2 were exposed to simulated PWR primary water at 340 °C for 500 h in a 23 liter 316L stainless steel autoclave. The nominal composition of the simulated environment was made of 1000 mg/L H_3BO_3, 2 mg/L LiOH. Partial hydrogen pressure of 30 cc dissolved Hydrogen per kg H_2O was measured by a Ag/Pd probe during the test. The remaining samples from sets H1 and H2 were exposed for 500 h in the autoclave in steam at 400 °C – and at 200 bar.

2.2. Surface characterization

For TEM and electron energy loss spectroscopy (EELS) analyses, cross-sections of the oxide layer were prepared by cutting the samples into thin slices (normal to the oxide/substrate interface) with a diamond wire saw. Two slices were glued together, oxide to oxide, and embedded in a 3 mm diameter brass tube in epoxy resin. After curing, the tube was sectioned into approximately 300 μm thick discs. These discs were then polished on both faces and dimpled before ion-milling to transparency with a low angle (0–10°) precision ion-beam polishing system (PIPS). TEM investigations were done using a JEOL JEM 2010 microscope operated at 200 kV and equipped with an energy dispersive spectrometer (EDS) for chemical analysis at University Paul Sabatier Temscan Service (Toulouse, France). The EEL spectra were carried out using a FEI TECNAI microscope with a GIF TRIDIEM at Amiens University. The measurements presented in this study were done at a total energy resolution of 0.8 eV as determined from the full width at half maximum of the zero-loss peak. The following conditions were chosen to acquire the EELS spectra: an illumination semi-angle α of 1.9 mrd, a collection semi-angle β of 3.25 mrd and an energy dispersion of 0.1 eV/channel. The energy positions of the Fe, Cr–$L_{2,3}$ and O–K edges were accurately determined using the internal calibration system based on the electrostatic drift tube of the EELS spectrometer.

Diffusion profiles of chemical elements or oxides from base metal to oxide layer were determined by Reverse – SIMS analyses. It consists of the erosion of the sample surface with a beam primary ion of energy (here 10 keV Cs^+) to produce ionized secondary particles, subsequently detected by a mass spectrometer. The equipment, a CAMECA IMS 4F6 is located at the physics department of INSA Toulouse (France). Specimens to be analyzed were glued to a brass sampler so that the oxide was against the sampler. The sample was then ground by SiC papers (600–4000 grades) until sample thickness was less than 20 μm and the surface at the base metal side was polished to a mirror using diamond pastes. The thin section was then released from the sampler and was ready for analysis.

3. Results

In order to characterize the oxidation products, optical microscopy and TEM coupled to EELS were performed on 304L SS austenitic samples with the two different surface preparation treatments, exposed to steam (400 °C, 500 h) or simulated PWR environment (340 °C, 500 h). The results are first described for oxidation in steam (400 °C, 500 h) and then in the simulated PWR environment.

3.1. Exposure to steam environment (400 °C , 500 h)

3.1.1. Polished samples (mechanical polishing)

A cross section showing the oxide layer is reported in Fig. 1. The cross section shown in Fig. 1 reveals that the oxide layer is composed of large, facetted crystallites (dotted 1 and 2 on Fig. 1a) with size that can reach 1 μm and of crystallites of smaller size (dotted 3, 4 and 5 on Fig. 1a) ranging from 70 to 100 nm and distributed between the biggest crystallites. EDX analyses of the big crystallites gave a chemical composition of 56 at% of O, 39 at% Fe, 3 at% Cr and 2 at% Ni. A

Table 1
Chemical composition of the 304L SS (wt.%).

Element	Pb	W	Zr	S	P	C	B	Mg	N	Co	Si	Cu	V	Mo	Mn	Ti	Ni	Cr	Fe
304L_GV 20	8 ppm	0.035	12 ppm	0.002	0.01	0.012	–	0.003	–	<0.05	0.45	0.24	0.015	0.02	1.65	<0.05	8.55	18.75	Bal.

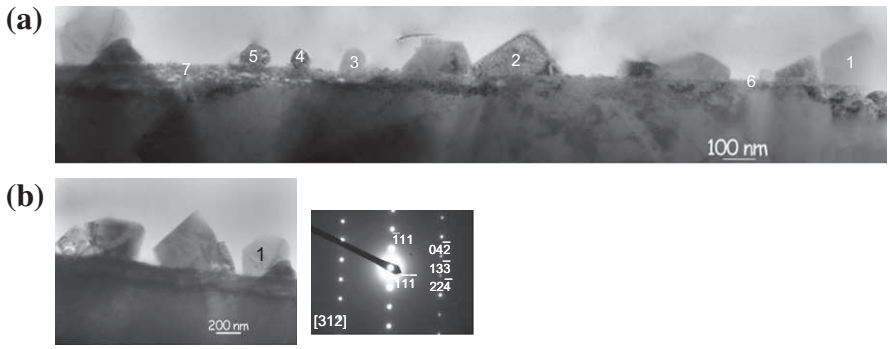

Fig. 1. Cross section of the oxide layer of 304L (H1) after 500 h exposure to steam environment (400 °C) (a) bright field image of oxide layer of 304L (crystallites dotted 1 and 2: magnetite, dotted 3, 4 and 5: $FeCr_2O_4$ and area dotted 6 and 7: Cr-rich layer (b) crystallite of magnetite associated with its diffraction pattern (zone axis [3 1 2]).

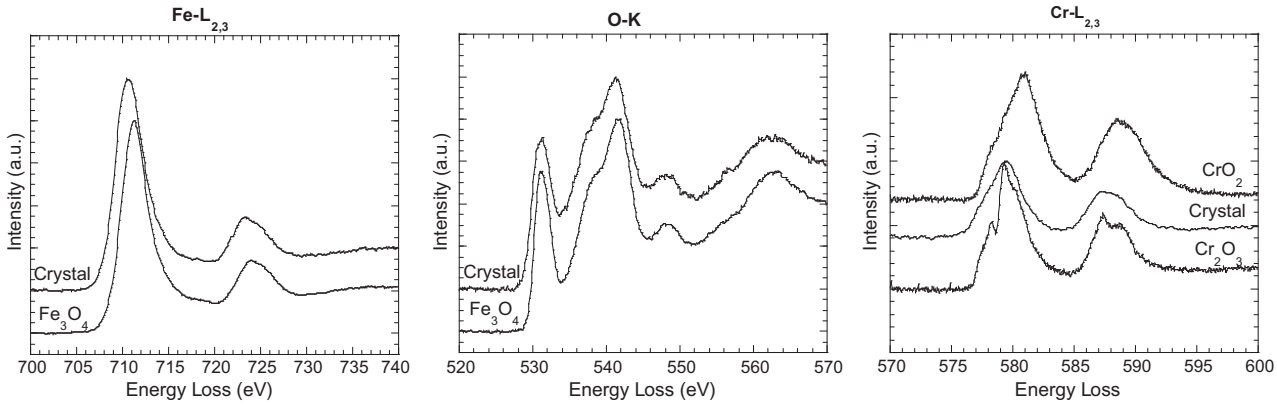

Fig. 2. Fe–$L_{2,3}$, O–K and Cr–$L_{2,3}$ EELS spectra on crystallites pointed 3, 4 and 5 on Fig. 1 associated with reference spectra obtained in the same experimental conditions of Fe_3O_4, CrO_2 (Cr^{4+}) and Cr_2O_3 (Cr^{3+}).

different chemical composition was obtained for the smaller crystallites: a lower proportion of iron (29 at% of Fe), a higher proportion of chromium (13 at% of Cr) and similar percentages of nickel and oxygen. An electronic diffraction pattern of crystallites 1 and 2 confirmed the magnetite phase (space group: Fd-3 m, a = 8.41 Å). The exact nature of the smaller crystallites was determined from the EELS spectra. Fig. 2 shows that these crystallites display a position in energy and a signature on the Fe–$L_{2,3}$ and O–K edges that is modified compared to the magnetite signature (Fig. 2).

The energy position of Fe–$L_{2,3}$ is characteristic of the iron signature at an oxidation state of +2. The O–K edge did not present an energy shift. Nevertheless, the first peak localized at 531 eV shows a surface area different than those of magnetite; this indicates a difference in chemical environment. Moreover, for the Cr–$L_{2,3}$ edge (Fig. 2), the energy position is identical to that of chromium at oxidation state +3, but the fine structure is different from those obtained for Cr_2O_3. It was then concluded that the composition of these crystallites was very close to spinel $Fe^{2+}Cr^{3+}_2O_4$.

Due to EDX analysis, chromium concentration increased in the oxide until the oxide/substrate interface (50–60 at%). The oxide layer was inhomogeneous along the surface as shown by the dotted areas 6 and 7 in Fig. 1, with a thickness which can reach 100 nm (dotted 7 on Fig. 1) and is composed of small crystallites revealed by HRTEM (High resolution TEM). The STEM EELS analyses on this area reveal the same spectra as that of the small crystallites described above, i.e. the same spinel $Fe^{2+}Cr^{3+}{}_2O_4$ composition. Fig. 3 shows the distribution of iron, chromium and oxygen obtained by EFTEM for an area of Fig. 1 (crystallites dotted 3, 4 and 5).

The oxygen map (Fig. 3b) shows the distribution of oxygen at the surface of the sample and confirms the presence of the outer and inner part of the oxide layer. Moreover the chromium and iron map clearly shows chromium enrichment on the inner part of the oxide.

Finally, EDX analysis of the substrate showed an increase in chromium content through a thickness of 1 μm and the chemical composition of the bulk was found after 1.5 μm.

3.1.2. Precision ground samples

Quick analysis by optical microscopy showed the presence of crystallites at the surface and in the streaks left by the precision grinding. An overview obtained by TEM is given in Fig. 4.

This overview displays the same oxide layer morphology as that observed for the polished sample: an outer and an inner oxide layer. However the biggest Fe_3O_4 crystallites were smaller than 500 nm and few were observed on the free surface. The other crystallites presented a chemical composition corresponding to the $FeCr_2O_4$ spinel (based on STEM EELS studies not shown here) and formed a compact layer about 50 nm thick. The chromium enriched layer at the oxide/substrate interface was very thin, about 5–10 nm. The substrate presented a disordered layer of 1.5 μm thickness composed of small crystallite grains (size ~100 nm). The diffraction pattern obtained in this substrate is characteristic of a fine crystallized area and can be indexed using the inter-reticular distance of austenitic iron (a = 3.60 Å). No enrichment of chromium was observed at the oxide/substrate interface. After this 1.5 μm disturbed thickness, a normal grain distribution was observed in the substrate.

In conclusion for steam oxidation, the oxide layer was thicker for polished samples than for ground samples. Similarly, the protective inner layer rich in chromium can reach 100 nm thickness

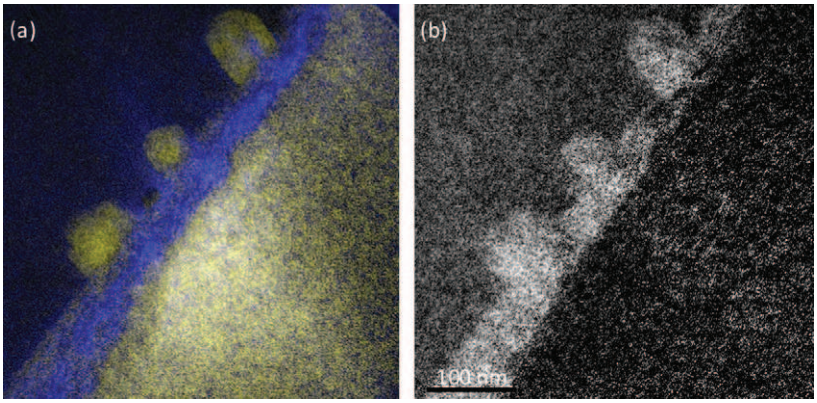

Fig. 3. EFTEM analysis (a) iron: yellow – chromium: blue (showing the chromium enrichment on the inner part of the oxide) and (b) oxygen map showing the outer and inner part of the oxide layer. (For interpretation of the references to color in this figure legend, the reader is referred to the web version of this article.)

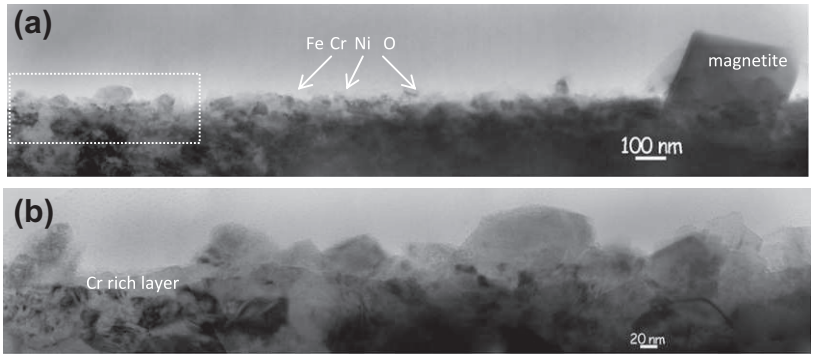

Fig. 4. Bright field image of oxide layer of 304L (H2) (a) overview and (b) high magnification image showing the $Fe(Cr/Ni)_2O_4$ crystallites and the Cr-rich layer.

for polished samples while for ground finished sample, it was only 5–10 nm.

3.2. Exposure to simulated PWR primary water (340 °C, 500 h)

3.2.1. Polished samples (mechanical polishing)

Fig. 5a shows an overview of the cross section of the oxide obtained after 500 h in primary PWR water at 340 °C. The oxide layer is composed of two layers: the biggest crystallites not present in Fig. 5a are sparsely dispersed over the surface. Their size can reach 1 μm and their chemical composition is closed to Fe_3O_4. The diffraction pattern study confirms the magnetite phase. However, these large crystallites were not numerous and the other crystallites were sized from 50 to 100 nm with a composition near that of spinel $Fe(Cr/Ni)_2O_4$. The compact oxide layer rich in chromium presented an inhomogeneous thickness which varied between 50 and 200 nm. In the substrate, near the substrate/oxide interface, strong enrichment of nickel (depletion of chromium) was observed. EDX analysis (not shown here) showed that the thickness of Cr depletion was around twice that of the Cr oxide layer. The presence of elongated nano-sized grains within the first 400–500 nm of the substrate is shown in Fig. 6.

3.2.2. Precision ground samples

An overview of the oxide layer is shown in Fig. 5b. The oxide occurs as a small quantity of large crystallites dispersed across the surface, sized from 300 to 700 nm (not shown in Fig. 5b). The diffraction pattern obtained for these crystallites is characteristic of the spinel phase Fe_3O_4. Crystallites of smaller sizes (from 20 to 40 nm) (shown in Fig. 5b) are dispersed around the larger ones. Below the crystallites, a thin layer (~10 nm thick) is enriched in chromium. At the substrate/oxide interface, the substrate presents a

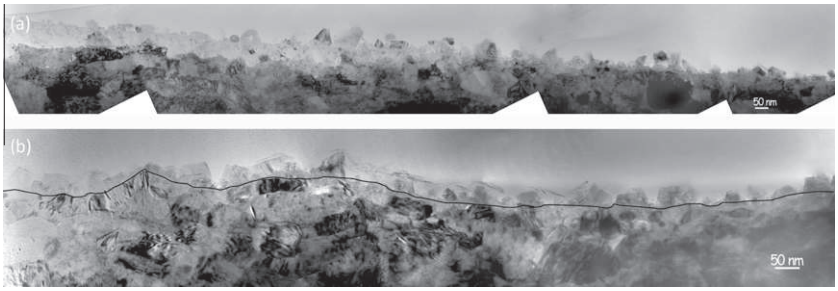

Fig. 5. Bright field images of 304L after 500 h exposure to simulated PWR primary water (340 °C) (a) mechanical polishing surface preparation (H1) and (b) finishing ground surface (H2).

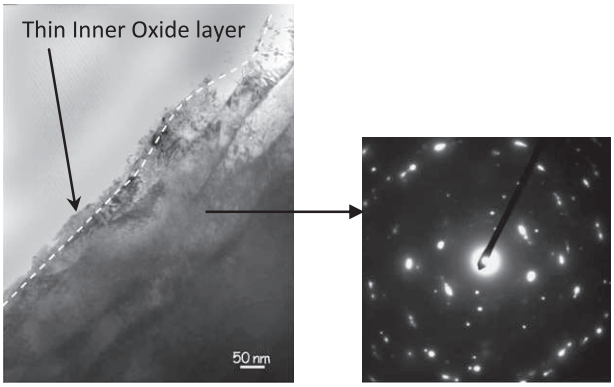

Fig. 6. Bright field image of one area of a TEM specimen showing elongated nanograins in the substrate and a specific diffraction pattern of the recrystallized area.

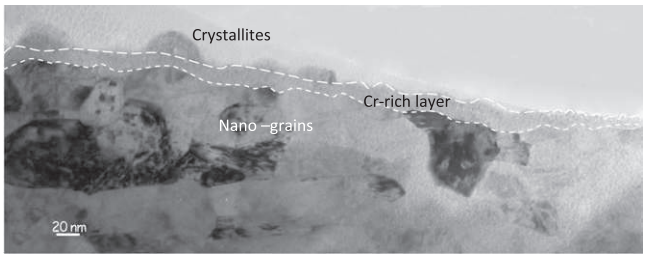

Fig. 7. Bright field image of the oxidized 304L (aerated oven 500 h at 400 °C) showing the crystallites, the Cr-rich layer and the nano-grains substrate.

layer of nano-crystallized grains 1.5 μm thick. The oxide/substrate interface presents enrichment in nickel but the substrate rapidly recovers the normal chemical composition.

In conclusion, for samples exposed in PWR environment, the oxide layer is thicker for polished samples than for finishing ground ones. The protective layer rich in chromium can reach 100 nm for polished sample even though its thickness is only 10 nm for ground samples. Origin of the recrystallized area observed in steam and aqueous environment has been investigated through a ground 304L sample before any exposure. The surface of this sample is composed of a nano-crystallized grain layer 1 μm thick and contains no oxygen. Moreover, this ground sample was exposed in an aerated oven at 400 °C for 500 h. The oxide cross section (Fig. 7) shows that below the oxide layer, the substrate also presents a nano-crystallized grain layer 1 μm thick and contains oxygen down to 500 nm of thickness. It is then concluded that this area results from surface preparation and is not due to exposure in environment.

4. Discussion

Oxidation of Austenitic Stainless Steel 304L in aqueous environment implies electronic exchanges (i.e. electrochemical reactions) and ionic species transportation between base metal and the environment. According to Refs. [2,6,7,9], 304L ASS oxidation in an aqueous environment leads to an oxide layer made up of an outer layer composed of magnetite crystallites (Fe_3O_4) and a compact inner layer, the interfacial layer. Moreover, spinels enriched in iron and chromium depending on the stoichiometry ($FeCr_2O_4$ spinels type) may be disposed on the inner and outer layer. Inner and outer layer's characteristics are quiet different, in terms of composition, crystallite structure and conductivity. These studies show that the chromium content increases from the outer layer to the interfacial layer.

The present results are in agreement with those obtained in a 316L steel [7] where the presence of a double layer oxide, a coarse outer layer composed of Fe_3O_4 crystallites and an inner layer with some fine $FeCr_2O_4$ spinel (10 nm) was reported. Simplification schemas of the oxides observed in the present study are displayed in Fig. 8. In high temperature steam or in simulated PWR environment and for both surface preparations, the oxide layer is in a duplex configuration. This oxide film is composed of the **outer oxide layer** composed of magnetite crystallites and $FeCr_2O_4$ or $Fe(Cr/Ni)_2O_4$ spinel type, crystallized and disposed in the **interfacial layer also named the inner layer**, which is thin, compact, and rich in chromium. A similar oxide structure was observed in a sample removed from steam generator channel heads at the Beznau I Nuclear power plant in Switzerland [9]. The specimens were exposed to PWR primary water. However, most of studies in the literature do not highlight the structure of the base metal at the subsurface. Characterization of the oxide sublayer is important, because it provides indications about diffusion paths available for species of concern during oxide formation. This characterization also allows the determination of potential oxide penetrations under the oxide layer and their localizations.

Our study shows the presence of a recrystallized area under the oxide layer. The diffraction pattern exhibiting a series of bright concentric rings specific to the non-structured area (actually constituted of nanograins) is represented in Fig. 6. This area was observed for two oxidation conditions (high temperature steam and simulated PWR) for both ground and polished samples surfaces.

Few studies report recrystallization of metal under the oxide layer. Grain boundary corrosion in heavily deformed and recrystallized surface substructures accompanied with IGSCC was pointed out in [18] where two 316L heats were characterized after service exposure in PWR and BWR environment. The recrystallized area is displayed as elongated fine grains with high dislocation density under the surface oxide. According to the authors, EBSD (Electron Back Scattered Diffraction) analyses indicate that local strain gradients below the surface lead to recrystallization conditions under the oxide layer. This substructure is correlated with the presence of penetrative intergranular corrosion/oxidation throughout the nanocrystalline microstructure. Carette [19] reported this recrystallized area on an 600 alloy oxidized in PWR environment.

The penetration of chemical elements penetrations into the oxide sublayer was also characterized in the present study. Reverse SIMS characterizations were performed for two 304L SS samples (one polished and the other ground) exposed to simulated PWR primary water. The resulting composition profiles of elements (^{16}O, ^{12}C) and oxides (^{16}OTi, ^{16}OCr, ^{16}OAl and ^{16}ONi) are displayed in Fig. 9, which plots intensity signal versus depth, from base metal to oxide layer. A deeper depth has been studied in the metal for Fig. 9a than those of Fig. 9b. For a polished sample, oxide intensities (Al, Ti, Fe, and Ni) were regular along the base metal and show a sharp increase in the outer oxide layer. No singularities are observed in the different oxide profiles or the ^{12}C profile (marking oxidation of carbides in the base metal). However, the ^{16}O profile and $^{27}Al^{16}O$ profile exhibits a singularity in the base metal, far from oxide (circled in Fig. 9a and b). This may be linked to the presence of aluminum oxides dispersed in the metal matrix. Diffusion profiles are similar for ground surface preparation, in particular for aluminum oxide. However, it should be recalled that aluminum is a thermodynamically reactive element and reacts with oxygen in high temperature water where it is preferentially oxidized.

From the results of this study, it appears there is no evidence of oxide penetration or intergranular oxidation in a simulated PWR environment for 304L. Unlike in [18] where samples are polished or ground (initial surface highly deformed) and exposed to LWR primary water, there was no accelerated localized corrosive attack or penetrative oxidation through deformed and recrystallized sub-

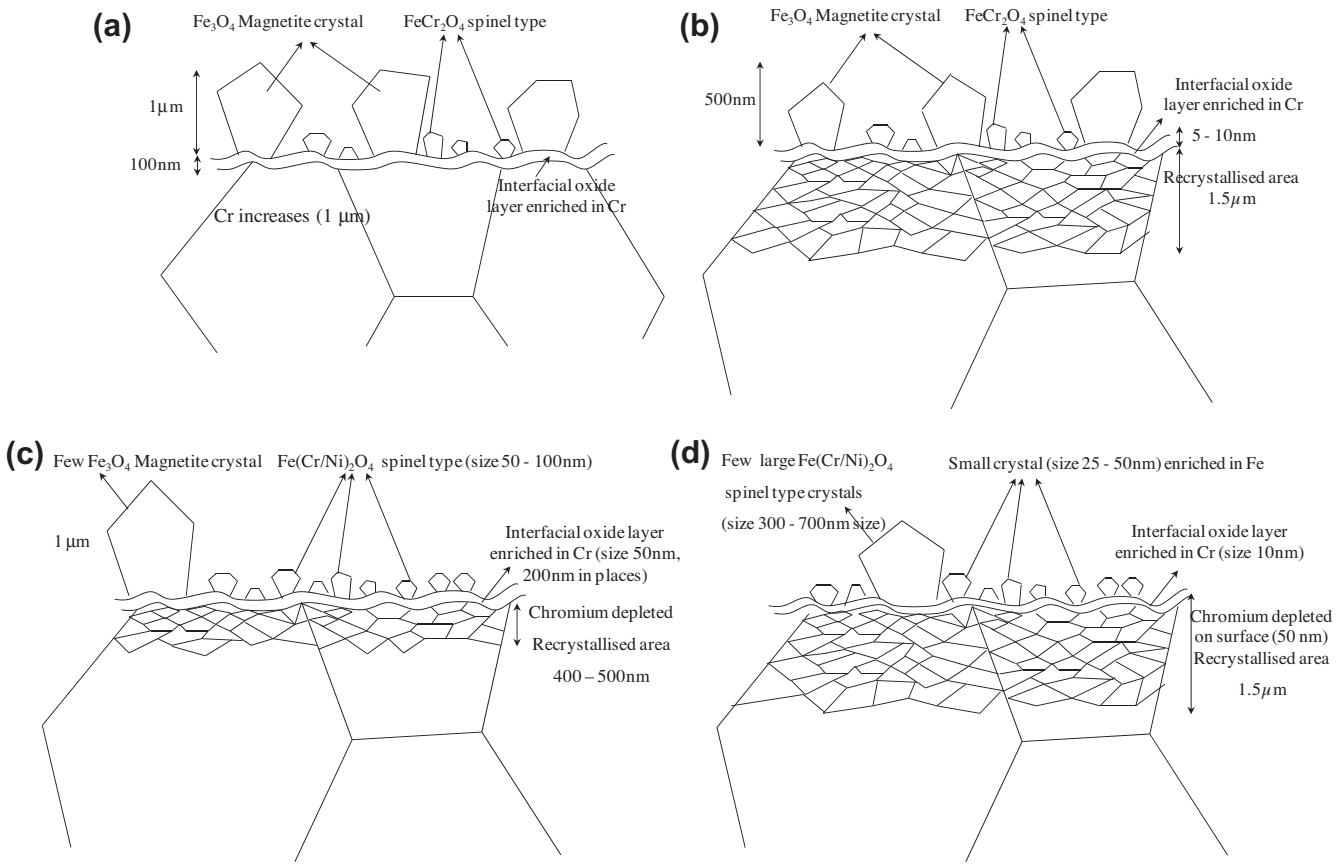

Fig. 8. Schematic representation of the oxide formed on a 304L sample (a) polished and exposed to 400 °C steam – for 500 h, (b) ground and exposed to 400 °C steam for 500 h, (c) polished and exposed to 340 °C simulated PWR primary water – for 500 h and (d) ground and exposed to 340 °C simulated PWR primary water for 500 h.

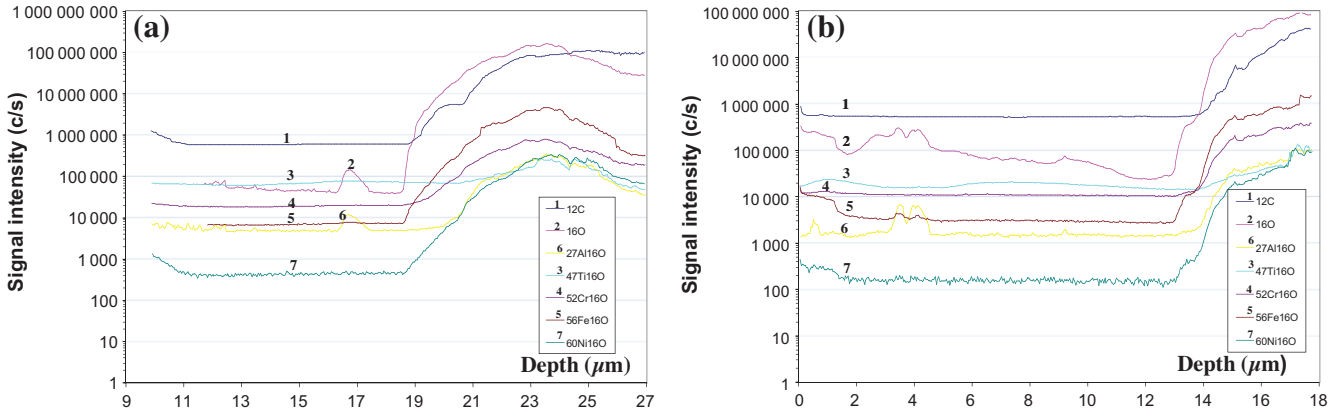

Fig. 9. Composition profile of elements (^{16}O, ^{12}C) and oxides (^{16}OTi, ^{16}OCr, ^{16}OAl and ^{16}ONi) versus depth (from base metal (left side) to the oxide layer) obtained by reverse SIMS for (a) polished sample exposed to PWR environment and (b) ground sample exposed to PWR environment (circled highlights showing the presence of aluminum oxides dispersed in the metal matrix) – a deeper depth has been studied in the metal for (a) than for (b).

structures. However, the thickness of the recrystallized area is directly linked to the surface preparation: when the sample is polished, the recrystallized area is missing (steam environment) or thin (500 nm PWR environment) while when the surface is ground, the recrystallized area is much thicker (1.5 µm for steam or PWR environment and 1 µm for air environment). According to [10], surface preparation (whether grinding or polishing) produces significant subsurface deformation including high dislocation densities, phase transformations (not in our study) and recrystallization as shown in Fig. 8. Thus, surface preparation may modify surface structure and that is one indication of crucial issue that represents surface treatment of samples in laboratory oxidation studies.

4.1. Accelerating effect of steam on austenitic stainless steel oxidation

The duplex structure observed in the sample exposed to high temperature steam is actually similar in nature to that obtained in sample oxidized in simulated PWR primary water. Oxidation kinetics in reactor water was slower than that of the steel in steam, given that passive film formed during 500 h exposure in steam at

400 °C was thicker than that formed during 500 h exposure in simulated PWR water at 340 °C. To uncouple the effect of temperature on oxide growth from that of the environment, exposure in PWR primary water at 340 °C was led and the oxide layer is also almost thinner than that formed in steam environment. This experiment indicates that in this range, the temperature effect seems negligible for steam/water comparison in terms of oxide thickness. The more noticeable difference between steam or the PWR environment exposure is then, linked to chromium enrichment of the substrate when the sample is exposed to high temperature stream while the substrate is depleted in chromium (enrichment of nickel) after PWR environment exposure. This suggested that the PWR environment may lead to oxide penetrations into the substrate, precisely at grain boundaries. This was validated by Bruemmer [18], who reported intergranular penetrations for a 316L core exposed to BWR and PWR environments. From this, it appears that kinetic diffusion of species involved in passive film formation in steam may not be suitable for oxide development in oxide sub layer. However, the SIMS studies performed in the present work did not give evidence of oxide penetration in 304L SS exposed to simulated PWR.

4.2. Influence of surface treatment on the type of oxide formed

Surface preparation is a key issue in SCC literature. In order to determine the effect of surface treatment on the generalized corrosion of our steel, two surface preparations were studied: polishing and grinding.

For exposure to high temperature steam, the nature of the oxide formed was similar for the two surface treatments. The oxide was twice as thick for the polished surface than for precision grinding; this observation is in agreement with that of Warzee et al. [20]. A similar conclusion was also reached by Tapping et al. [8]. The trend was similar for the protective layer rich in chromium: it reached 100 nm for the polished sample but only 10 nm for the ground one. These conclusions suggested that the diffusion of species involved in electrochemical reaction such as Cr^{3+} is faster for polished than for ground surfaces. Actually, the main difference between these two kinds of surface is the thickness of the recrystallized area (see previous section) which is promoted by finishing grinding. Finally, the finer the grains, the shorter the grain boundaries, the poorer the diffusion paths, and the thinner is the oxide layer. That seems to be in agreement with Robertson's oxidation model, which is based on the diffusion of species through grain boundaries [6].

In general, oxide characterization studies in laboratories use polished samples to uncouple surface treatment effects from the mechanisms effectively taking place during oxidation. Actually, under normal service conditions, components of nuclear reactor vessels are not polished so the oxide layer formed is thinner than that formed in laboratory conditions.

5. Conclusions

This work concerns the study of corrosion behavior of an 304 ASS in high temperature steam (400 °C, 500 h) and in PWR environment (340 °C, 500 h) as well as the effect of surface preparation. The following conclusions were reached:

1. A duplex oxide layer is formed during exposure of 304L SS in high temperature water and steam. This layer is composed of an inner compact layer rich in chromium and an outer layer presenting large crystallites of magnetite (Fe_3O_4) and smaller spinels enriched in iron and chromium ($Fe(Cr, Ni)_2O_4$ spinels type). This result is in agreement with previous studies [3–11].
2. The base metal beneath the oxide layer is recrystallized and the substructure is composed of fine elongated nanograins. Irrespective of the environment, the thickness of this layer depends on surface roughness. A polished surface exhibits a thin recrystallized area, which is twice or three times as thick when surface is ground. In parallel, the oxide layer is thinner, when the recrystallized area formed is thicker (ground surface). Thus, surface preparation by polishing promotes development of the oxide layer. These observations seem to indicate that oxide growth is based on diffusion of species through grain boundaries in agreement with the Robertson oxidation model [6]. Quantitative studies such as diffusion rates of species of concern in different diffusion paths or corrosion rate determination should enable us to refine this hypothesis.
3. Steam accelerates corrosion kinetics of 304L SS compared with the aqueous environment. It reproduces a similar oxide layer but thicker than that produced in a PWR environment. However, the base metal underlying the oxide layer is impoverished in chromium for samples exposed to the PWR environment, unlike in samples exposed to steam (where the sublayer is enriched in chromium). Diffusion processes may be different in the two environments.

Acknowledgments

We gratefully acknowledge C. Guerre from SCCME (CEA Saclay) for providing the autoclaves, V. Amicel for his assistance in the exposure of samples in the two environments and P. Bonaillie (SRMP CEA Saclay) for SEM characterizations.

References

[1] M.C. Bloom, C.N. Newport, W.A. Fraser, Steel corrosion mechanisms, J. Electrochem. Soc. 111 (1964) 1343–1347.
[2] E.C. Potter, G.M.W. Mann, Oxidation of mild steel in high-temperature aqueous systems, in: Proceedings of the 1st International Congress of Metallic Corrosion, London, 1961, Butterworths, 1962, p. 417.
[3] D.H. Lister, R.D. Davidson, E. McAlpine, The mechanisms and kinetics of corrosion product release from stainless steel in the lithiated high temperature water, Corros. Sci. 27 (1987) 113–140.
[4] J.E. Castle, H.G. Masterson, The role of diffusion in the oxidation of mid steel in high temperature aqueous solutions, Corros. Sci. 6 (1966) 93–101.
[5] S.E. Ziemniak, M. Hanson, Corrosion behaviour of 304 stainless steel in high temperature hydrogenated water, Corros. Sci. 44 (2002) 2209–2230.
[6] J. Robertson, The mechanism of high temperature aqueous corrosion of steel, Corros. Sci. 29 (1989) 1275–1291.
[7] T. Terachi, K. Fujii, K. Arioka, Microstructural characterization of SCC crack tip and oxide film for SUS 316 stainless steel in simulated PWR primary water at 320 °C, J. Nucl. Sci. Tech. 42 (2005) 225–232.
[8] R.L. Tapping, R.D. Davidson, E. McAlpine, D.H. Lister, The composition and morphology of oxides formed on 304 stainless steel in lithiated high temperature water, Corros. Sci. 26 (1986) 563–576.
[9] P. Aaltonen, K. Makela, H. Venz, H.P. Meier, X-ray diffraction characterization of oxide films on the primary circuit surfaces at Beznau Unit 1, in: Proceedings of EUROCORR-98, Utrecht, Netherlands, 1998, p. 110.
[10] S. Lozano-Perez, D.W. Saxey, T. Yamada, T. Terachi, Atom-probe tomography characterization of the oxidation of stainless steel, Scripta Mater. 62 (2010) 855–858.
[11] T. Couvant, P. Moulart, L. Legras, P. Bordes, J. Capelle, Y. Rouillon, T. Balon, PWSCC of austenitic stainless steels of heaters of pressurizers, in: Proceedings of the 13th International Conference Environmental Degradation of Materials in Nuclear Power Systems–Water Reactors, CNS, CDROM, 2007.
[12] B. Stellwag, The mechanism of oxide film formation on austenitic stainless steels, Corros. Sci. 40 (1998) 337–370.
[13] A. Turnbull, K. Mingard, J.D. Lord, B. Roebuck, D.R. Tice, K.J. Mottershead, N.D. Fairweather, A.K. Bradbury, Sensitivity of stress corrosion cracking of stainless steel to surface machining and grinding procedure, Corros. Sci. 53 (2011) 3398–3415.
[14] S.J. Lee, J.J. Lai, The effects of electropolishing (EP) process parameters on corrosion resistance of 316L stainless steel, J. Mater. Proc. Tech. 140 (2003) 206–210.
[15] H.S. Lee, D.S. Kim, J.S. Jung, Y.S. Pyoun, K. Shin, Influence of peening on the corrosion properties of AISI 304 stainless steel, Corros. Sci. 51 (2009) 2826–2830.
[16] V. Zatkalikova, T. Liptakova, Pitting corrosion of stainless steel at the various surface treatment, Mat. Eng. 18 (2011) 115–120.

[17] S. Daopiset, N. Karnchanaprayut, N. Kiatsareekul, T. Kongkrapan, Effects of surface finishes on corrosion resistance of welded stainless steels, AIJSTPME 3 (2010) 65–71.
[18] S. Bruemmer, Surface Damage and Environment-Assisted Cracking Precursors in LWR Components in SCC Initiation Workshop, Beaune, Bourgogne, France, 2008.
[19] F. Carrette, Relâchement des produits de corrosion des tubes en alliage 690 de générateur de vapeur du circuit primaire des réacteurs à eau pressurisée, Institut National Polytechnique de Toulouse, Toulouse, thesis, 2002.
[20] M. Warzee, J. Hennaut, M. Maurice, C. Sonnen, J. Waty, Ph. Berge, Effect of surface treatment on the corrosion of stainless steels in high temperature water and steam, J. Electrochem. Soc. 112 (1965) 670–674.